Cooperative Behaviour of Semiflexible Polymers and Filaments

Jan Kierfeld, Pavel Kraikivski, Torsten Kühne, and Reinhard Lipowsky

Max Planck Institute of Colloids and Interfaces, Science Park Golm, 14424 Potsdam, Germany

Summary. Semiflexible polymers and filaments play an important role in biological and chemical physics. The cooperative behaviour of interacting filaments and the internal bending modes of a single filament give rise to various equilibrium phase transitions, such as bundling and adsorption, which are reviewed in this article. In motility assays, filaments are adsorbed and driven by motor proteins, which are anchored to a planar two-dimensional substrate. We present a simulation model for the active filament dynamics in this non-equilibrium system.

1 Introduction

Stiff, filamentous polymers play an important role in biological and chemical physics. Such polymers have a considerable bending rigidity, which gives rise to persistence lengths comparable to or larger than their contour lengths. These semiflexible polymers exhibit a variety of cooperative phenomena, which we want to discuss in this article. These transitions result from the competition of several energies in the system, i.e., the bending energy, the thermal energy, interaction energies, and external driving forces. In biological systems, driving forces can arise from the activity of molecular motors which perform directed walks on cytoskeletal filaments.

First we will discuss the equilibrium phase transition that leads to the formation of filament bundles in the presence of attractive interactions, which can arise from crosslinking proteins or unspecific interactions [3]. In eukaryotic cells, the most important building blocks of the cytoskeleton are microtubules and filamentous actin (F-actin). Actin filaments have a persistence length $L_p \simeq 30\mu m$ [1], microtubules are much stiffer with a persistence length $L_p \sim mm$ [2]. In the cortex of the cell, actin filaments form a dense meshwork which is responsible for many of the viscoelastic properties of the cell. Another important morphology that is found in the cell are filament bundles [4], which, e.g., support cell protrusions and serve as stress fibres. Both meshworks and bundles are hold together by different actin-binding crosslinking proteins [4, 5].

Actin bundling crosslinkers possess two adhesive end domains which bind to filaments by weak bonds; crosslinker mediated interactions therefore allow a reversible formation of actin bundles, which can be regulated by the concentration of crosslinkers in solution. Solution of actin filaments and crosslinking proteins have been studied *in vitro* in a number of recent experiments [6–8]. In these studies it has been observed that bundle formation in F-actin solutions containing crosslinking molecules requires a threshold crosslinker concentration above which F-actin bundles become stable against the thermal fluctuations of filaments and a phase containing networks of bundles separates.

Another important equilibrium phase transition of polymers is their adsorption to an attractive planar surface. For semiflexible polymers or filaments, the adsorption transition is similar to the binding of two filaments but represents a distinct universality class [9]. Various single molecule methods have been applied to adsorbed semiflexible polymers because both visualization and manipulation are easier for adsorbed polymers with a large diameter, such as DNA [10, 11]. These polymers are generically semiflexible because stronger entropic or enthalpic interactions along their backbone increase the bending rigidity. The thermally activated dynamics of single filaments adsorbed on structured substrates has been discussed in Refs. [12]. Here, we will focus on the adsorption behaviour of filaments in motility assays. In such an assay, cytoskeletal filaments are adsorbed and driven over a two-dimensional, planar substrate by motor proteins whose tails are anchored to the substrate [13]. In order to obtain adsorption, a critical density of motor proteins is needed in close analogy to the critical crosslinker concentration for the formation of a filament bundle.

Motility or gliding assays are a standard biochemistry assay to characterize motor proteins, which is based on measuring the active dynamics of adsorbed filaments. In biological cells, small forces generated by motor proteins organize and rearrange cytoskeletal filaments and give rise to active, non-equilibrium filament dynamics, which plays an important role for cell division, motility, and force generation [17]. Whereas conventional "passive" polymer dynamics is governed by thermal fluctuations [18], active filament dynamics is characterized by a constant supply of mechanical energy by motor proteins, which hydrolyze adenine triphosphate (ATP). Motility assays are model systems, which allow to study active filament dynamics in a controlled manner. By analyzing the transport velocities of *single* filaments gliding over the substrate, information can be obtained about basic properties of molecular motors such as their maximal velocity. We introduce a simulation model for motility assays, which refines previous models [14–16] and contains semiflexible filaments, motor heads, and polymeric motor tails as separate degrees of freedom.

This article is organized as follows. In section 2 the formation of filament bundles via crosslinker-mediated attractive interactions is discussed. The adsorption of a filament onto an adhesive surface is considered in section 3. In particular, we discuss the filament adsorption on a planar two-dimensional substrate covered with anchored motor proteins, which represents the geom-

etry used in motility assays. In section 4, we introduce a model for the active filament dynamics in motility assays and present recent simulation results.

2 Filament bundles

We consider N filaments with bending rigidity κ in a solution containing crosslinking molecules with two adhesive end groups. The persistence length of such a filament is $L_p = 2\kappa/T$, where T is the temperature in energy units. This system exhibits a critical crosslinker concentration, $X_1 = X_{1,c}$, which separates two different concentration regimes. For $X_1 < X_{1,c}$, the filaments are unbound and uniformly distributed within the compartment. For $X_1 > X_{1,c}$, the filaments form either a single bundle, which represents the true ground state of the system as in Fig. 1(a) and (c) , or several sub-bundles, which represent metastable, kinetically trapped states as in Fig. 1(b). Furthermore, as we decrease the crosslinker concentration from a value above $X_{1,c}$ towards a value below $X_{1,c}$, the bundles undergo a discontinuous unbinding transition at $X_1 = X_{1,c}$. The existence of a single, discontinuous unbundling transition can be established by analytic methods for $N = 2$ filaments [9] and by Monte Carlo (MC) simulations for larger bundles containing up to $N = 20$ filaments.

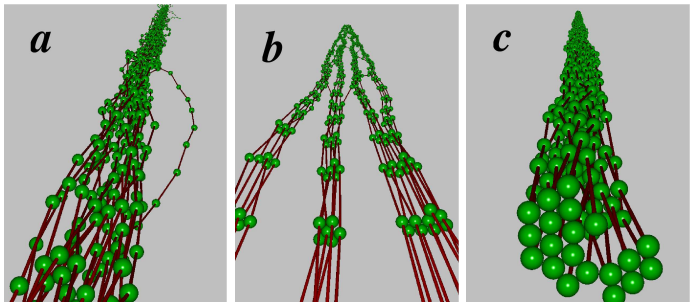

Fig. 1. Monte Carlo snapshots of bundles with $N = 20$ filaments. (a) Close to the unbinding transition in the bundled phase. (b) Deep in the bound phase, the bundle tends to segregate due to slow kinetics and filament entanglement. (c) The equilibrium shape of the bundle is roughly cylindrical.

2.1 Model

The filaments are oriented along one axis, say the x-axis, and can be parametrized by two-dimensional displacements $\mathbf{z}_i(x)$ $(i = 1, ..., N)$ perpendicular to the x-axis, with $0 < x < L$, where L is the projected length of the polymer. This parametrization is appropriate provided the longitudinal correlation length is small compared to L_p. We discretize the filament into segments of

length $a_\parallel$, i.e., $x_k = ka_\parallel$ and $\mathbf{z}_{i,k} = \mathbf{z}_i(x_k)$. The presence or absence of a crosslinker molecule at segment k of filament i is described by the occupation number $n_{i,k} = n_i(x_k) = 0, 1$. The filament-crosslinker system is described by the Hamiltonian

$$\mathcal{H} = \sum_i \left[\mathcal{H}_{b,i}\{\mathbf{z}_i\} + \mathcal{H}_1\{n_i\}\right] + \sum_{i,j} \mathcal{H}_2\{\mathbf{z}_i - \mathbf{z}_j, n_i, n_j\} \ , \tag{1}$$

where the first contribution $\mathcal{H}_{b,i} = \int_0^L dx \frac{1}{2}\kappa \left(\partial_x^2 \mathbf{z}_i\right)^2$ contains the bending energies of the filaments. The term $\mathcal{H}_1$ describes the intrafilament interactions of linkers. We consider a lattice gas of linkers with hard-core repulsion adsorbing on a filament with $\mathcal{H}_1 = \sum_k a_\parallel W n_{i,k}$ where $W < 0$ is the adhesive energy (per length) of one linker end group. The third contribution $\mathcal{H}_2$ describes the pairwise interactions between filaments i and j and is given by

$$\mathcal{H}_2 = \sum_k a_\parallel \Big[V_r(\Delta\mathbf{z}_{ij,k}) + \frac{1}{2}(n_{i,k} + n_{j,k} - 2n_{i,k}n_{j,k}) V_a(\Delta\mathbf{z}_{ij,k})\Big] \tag{2}$$

where $\Delta\mathbf{z}_{ij,k} \equiv \mathbf{z}_{i,k} - \mathbf{z}_{j,k}$. The first term is the hard-core repulsion of filaments that is independent of the linker occupation with a potential $V_r(\mathbf{z}) = \infty$ for $|\mathbf{z}| < \ell_r$ and $V_r(\mathbf{z}) = 0$ otherwise where ℓ_r is of the order of the filament diameter. The second term is the linker-mediated attraction and is non-zero if either segment k of filament i or segment k of filament j carries a linker. Then the other filament is attracted by a linker-mediated potential $V_a(\mathbf{z})$. The latter filament gains the additional energy $|W|$ if $|\Delta\mathbf{z}_{ij,k}| \leq \ell_a$, where the potential range ℓ_a is of the order of the linker size. This attraction is modelled by the potential well

$$V_a(\mathbf{z}) = W \quad \text{for } 0 < |\,\mathbf{z}| - \ell_r < \ell_a \ , \quad V_a(\mathbf{z}) = 0 \quad \text{otherwise.} \tag{3}$$

We can perform the partial trace over the crosslinker degrees of freedom $n_{i,k}$ in the grand-canonical ensemble to obtain an effective interaction between filaments. Each crosslinker has two adhesive ends. The first adhesive end adsorbs on a filament and establishes the standard Langmuir-type adsorption equilibrium with a linker concentration per site $X_1 \equiv \langle n_{i,k}\rangle_1 = Kc_x/(1 + Kc_x)$ where the average is taken with the Hamiltonian $\mathcal{H}_1$. X_1 is thus determined by the concentration c_x of linkers in solution, where K is the equilibrium constant of the association reaction of the crosslinker with the filament. Tracing over weakly bound linkers with $|W| \ll T/a_\parallel$, we end up with effective pairwise linker-mediated filament interactions, i.e., $\bar{\mathcal{H}}_2 \approx \frac{1}{2}\sum_k a_\parallel [V_r(\Delta\mathbf{z}_{ij,k}) + \bar{V}_a(\Delta\mathbf{z}_{ij,k})]$, which have the same functional form as the bare interactions; the short-range attractive part $\bar{V}_a$ is of the form (3) with a strength $\bar{W} \approx 2X_1 W$ proportional to the linker concentration on the filament. Pairwise filament interactions with potentials of the form (3) are generic and do not only arise from crosslinkers but also from van-der-Waals, electrostatic, or depletion forces.

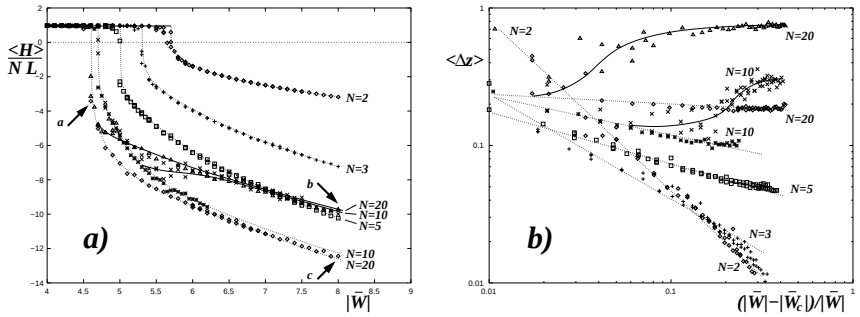

Fig. 2. MC data for $N = 2, 3, 5, 10, 20$ identical filaments (with persistence length $L_p = 200$, contour length $L = 100$, potential range $\ell_a = 0.001$, and hard core radius $\ell_r = 0.1$; all lengths are in units of Δx, lines are guides to the eye). For $N = 10, 20$ two branches of data are shown corresponding to two different initial conditions; in the lower branch we prepared a compact cylindrical configuration, in the upper branch (thick lines) we arranged filaments initially in a plane. (a) Mean energy $\langle \mathcal{H} \rangle / NL$ per filament (in units of T) as a function of the effective potential strength $|\bar{W}|$ (in units of $T/\Delta x$). Arrows correspond to the snapshots in Fig. 1. (b) Logarithmic plot of the mean filament separation $\langle \Delta z \rangle \equiv \langle |\Delta \mathbf{z}_{ij}| - \ell_r \rangle$ (in units of Δx) as a function of the reduced potential strength $(|\bar{W}| - |\bar{W}_c|)/|\bar{W}|$.

2.2 Discontinuous unbundling transition

We have studied bundle formation by MC simulations for up to $N = 20$ identical filaments ($\kappa_i = \kappa$) using the effective Hamiltonian $\mathcal{H} = \sum_i \mathcal{H}_{b,i} + \sum_{i,j} \bar{\mathcal{H}}_2$. The MC simulations can be used to determine the locus and order of the unbinding transitions, at which the mean energy $\langle \mathcal{H} \rangle$ exhibits a discontinuity, see Fig. 2a. To gain further insight into bundle morphologies, we also measure the mean segment separation $\langle |\Delta \mathbf{z}_{ij}| - \ell_r \rangle$, see Fig. 2b, which is directly proportional to the mean bundle thickness that can be determined by optical microscopy in experiments.

Our MC simulations confirm that, for bundles containing up to $N = 20$ filaments, there is a single, *discontinuous* unbinding transition, see Fig. 2a. In the presence of a hard-core repulsion, the critical potential strength $\bar{W}_c$ saturates to a N-independent limiting value for large N. As can be seen in Fig. 1a typical bundle morphologies close to the transition are governed by pair contacts of filaments. The bundle thickness, as given by the mean segment separation $\langle |\Delta \mathbf{z}_{ij}| - \ell_r \rangle$, stays *finite* up to the transition, see MC data in Fig. 2b. For increasing N, an increasing number of higher moments $\langle (|\Delta \mathbf{z}_{ij}| - \ell_r)^m \rangle$ remains finite at the transition [all moments $m < 2(N-1)(3N-4)/3$ remain finite] showing that the critical thickness fluctuations of large bundles become small.

Deep in the bundled phase, i.e., for large $|\bar{W}|$, our MC simulations show that bundles do not always reach their equilibrium shape. Small sub-bundles

containing typically $N \sim 5$ filaments form easily, start to entangle, and further equilibration is kinetically trapped suggesting that the bundle is in a "glass" phase. Fig. 1b shows the segregation into sub-bundles in a typical configuration and Fig. 2a shows the corresponding rise in the mean bundle energy per filament which approaches the $N = 5$ result. In Fig. 2b the pronounced rise of the mean separation for $N > 5$ with increasing potential strength and with increasing N is due to the segregation. This behaviour is reminiscent of the experimentally observed F-actin structures consisting of networks of small bundles [7]. Only when starting from a sufficiently compact initial state, bundles relax towards the equilibrium form in the MC simulation, which is a roughly cylindrical bundle with a hexagonal filament arrangement as shown in Fig. 1c. In contrast to the segregated form, the bundle thickness and the mean energy per filament of the equilibrium form decrease with increasing N, as can be seen in Fig. 2.

The critical potential strength $\bar{W}_c$ corresponds to a critical crosslinker concentration $X_{1,c}$. For weakly bound linkers $|W| \ll T/a_\parallel$, we have a simple linear relation $\bar{W} \approx 2X_1 W$ such that $X_{1,c} \approx \bar{W}_c/2W$. The corresponding relation for strongly bound linkers is more complicated.

Our simulations use periodic boundary conditions and treat very long and essentially parallel filaments. In order to include translational and rotational entropy we can map the ensemble of semiflexible filaments considered here onto an ensemble of rigid rods of finite length L and diameter $a_\perp$ at a certain concentration c. The effective pairwise attraction (per length) J is given by the bundling free energy of the filaments with $J \sim \bar{W}_c - \bar{W} > 0$ for $|\bar{W}| > |\bar{W}_c|$. Using the results of Refs. [19], we find that the hard rod system separates into a high-density nematic phase and a low-density nematic or isotropic phase above a critical attraction, which is in qualitative agreement with the experimental results in Refs. [6–8].

3 Filament adsorption

The adsorption transition of a single filament onto a planar substrate is qualitatively similar to the bundle formation for $N = 2$ filaments in 1+1 dimensions, where the one-dimensional perpendicular distance $z(x)$ from the surface is analogous to a one-dimensional separation between filaments. The adsorption transition can be solved analytically [9], which reveals that unbinding and desorption represent two distinct universality classes with different critical exponents.

Here we want to consider the adsorption of a filament with persistence length $L_p = 2\kappa/T$ on a planar two-dimensional substrate where molecular motors are adsorbed with an areal density σ. Each motor can bind to a filament within a capture radius w and a binding energy $W_m < 0$. In contrast to the case of the annealed crosslinker ensemble considered previously, the motors represent a *quenched* ensemble of adsorption points. In the following,

we consider the typical experimental situation of a rather uniform coverage with motor proteins and also neglect effects from filament fluctuations parallel to the surface. Then the array of motors gives rise to an average adsorption potential $\bar{V}_{ad}(z)$ of the same functional form as the potential (3) with a potential strength $\bar{W}_{ad} = W_m \sigma w$, the hard substrate at $\ell_r = 0$ and ℓ_a of the order of the capture radius w. On length scales comparable or smaller than L_p, the semiflexible polymer is only weakly bent by thermal fluctuations and its configurations are governed by the effective Hamiltonian

$$\mathcal{H}_{ad} = \int_0^L dx \left[\frac{\kappa}{2} (\partial_x^2 z)^2 + \bar{V}_{ad}(z(x)) \right] . \tag{4}$$

We consider the limit of long filaments $L\bar{W}_{ad} \gg T$, which can exhibit a desorption transition. Using the model (4), this desorption transition has been studied by transfer matrix techniques in Refs. [9]. The critical potential strength for desorption is $\bar{W}_{ad,c} = -cT/w^{2/3} L_p^{1/3}$ corresponding to a critical motor density $\sigma_c = T/W_m w^{5/3} L_p^{1/3}$, where $c \approx \sqrt{3\pi}/2 \approx 1.5$. For motor densities above this critical density, filaments adsorb onto the substrate with anchored motors against the thermal fluctuations of filaments. The critical motor density for adsorption is decreasing with increasing filament rigidity κ. The transfer matrix treatment shows that the free energy difference between adsorbed and unbound state vanishes as $|\Delta f| \approx |\bar{W}_{ad,c}||w|/\ln|w|^{-1}$ where $w \equiv (\bar{W}_{ad} - \bar{W}_{ad,c})/\bar{W}_{ad,c}$. Therefore, the correlation length $\xi_\parallel = T/|\Delta f| \propto |w|^{-\nu}$ diverges with an exponent $\nu = 1 + \log$. The weak bending approximation is valid as long as gradients are small, i.e., $\langle (\partial_x z)^2 \rangle \sim \xi_\parallel / L_p \lesssim 1$, which is fulfilled for $|\bar{W}_{ad} - \bar{W}_{ad,c}| \gtrsim T/L_p$, which typically applies to stiff filaments such as microtubules adsorbed by kinesins.

4 Motility assays for motor proteins

We consider a motility assay, where filaments are connected to the substrate by anchored motors of sufficient density $\sigma > \sigma_c$. In the presence of ATP, the motor heads start to perform a directed walk on the filaments, which induces active dynamics of adsorbed filaments.

4.1 Model

Our microscopic model for motility assays describes filaments, motor heads, and polymeric motor tails as separate degrees of freedom [22]. One end of the motor tail is anchored to the substrate and the motor head on the other end can bind to a filament in the correct orientation due to the tail flexibility. Once bound the motor head moves along the filament thereby stretching the polymeric tail, which gives rise to a loading force acting both on the motor head and the attached filament. This force feeds back onto the motion of the

bound motor head, which moves with a load-dependent motor velocity [20, 21]. Filaments follow an overdamped dynamics with external forces arising from the stretched motor tails and the repulsive filament-filament interaction.

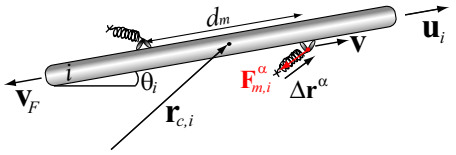

Fig. 3. Schematic top view of a filament i in the motility assay with two motors attached. The configuration of filament i is specified by the position $\mathbf{r}_{c,i}$ of its center of mass an its orientation angle θ_i; $\mathbf{u}_i = (\cos\theta_i, \sin\theta_i)$ is the orientational unit vector of the filament. $\mathbf{F}^{\alpha}_{m,i}$ is the force arising from the stretched polymeric tail of motor α, which has an end-to-end vector $\Delta\mathbf{r}^{\alpha}$. The polymeric tail is stretched by the motor head moving with velocity v, see eq. 6. d_m denotes the distance between attached motors.

To proceed, let us consider N rigid filaments of length L on a planar two-dimensional substrate [23]. The configuration of filament i ($i = 1, ..., N$) is then specified by the position of its center of mass $\mathbf{r}_{c,i}$ and its orientation angle θ_i, see Fig. 3. The overdamped translational and rotational dynamics of each filament i is described by stochastic Langevin-type equations of motion [22]

$$\begin{aligned} \boldsymbol{\Gamma} \cdot \partial_t \mathbf{r}_{c,i} &= \sum\nolimits_{\alpha=1}^{N_i} \mathbf{F}^{\alpha}_{m,i} + \sum\nolimits_{j=1}^{N} \mathbf{F}_{r,ij} + \boldsymbol{\zeta}_i \\ \Gamma_\theta \partial_t \theta_i &= \sum\nolimits_{\alpha=1}^{N_i} M^{\alpha}_{m,i} + \sum\nolimits_{j=1}^{N} M_{r,ij} + \zeta_{\theta,i} \ , \end{aligned} \tag{5}$$

where N_i is the number of motor heads attached to filament i and indexed by α. $\mathbf{u}_i = (\cos\theta_i, \sin\theta_i)$ is the orientational unit vector of filament i. $\boldsymbol{\Gamma}$ is the matrix of translational friction coefficients, $\boldsymbol{\Gamma} = \Gamma_\parallel \mathbf{u}_i \otimes \mathbf{u}_i + \Gamma_\perp (\mathbf{I} - \mathbf{u}_i \otimes \mathbf{u}_i)$ [18], where $\mathbf{I}$ is the unit matrix, and Γ_θ is the rotational friction coefficient. $\Gamma_\parallel$, $\Gamma_\perp$ and Γ_θ are the friction coefficients of the passive filament dynamics. $\boldsymbol{\zeta}_i(t)$ and $\zeta_{\theta,i}(t)$ are the translational and the angular components of the Gaussian distributed thermal random forces. $\mathbf{F}^{\alpha}_{m,i}$ is the force arising from the stretched tail of motor α. The end-to-end vector of the polymeric tail is $\Delta\mathbf{r}^{\alpha} \equiv \mathbf{r}^{\alpha}_i - \mathbf{r}^{\alpha}_0$, where the motor tail is anchored at $\mathbf{r}^{\alpha}_0$ and the head position is $\mathbf{r}^{\alpha}_i$. We model the polymeric tail as freely jointed chain such that $\mathbf{F}^{\alpha}_{m,i}$ is pointing in the direction $-\Delta\mathbf{r}^{\alpha}$ and its absolute value is obtained by inverting the force-extension relation of a freely jointed chain [24]. There is also a corresponding torque due to the motor activity, $M^{\alpha}_{m,i} = |(\mathbf{r}^{\alpha}_i - \mathbf{r}_{c,i}) \times \mathbf{F}^{\alpha}_{m,i}|$. The interaction forces $\mathbf{F}_{r,ij}$ and torques $M_{r,ij}$ are due to the purely repulsive interactions between filaments i and j corresponding to a hard-rod interaction for filaments of diameter D.

The dynamics of motor heads is described by a deterministic equation of motion, which has the form

$$\partial_t x_i^\alpha = v(\mathbf{F}_{m,i}^\alpha) \ , \tag{6}$$

where $|x_i^\alpha| \leq L/2$ defines the position of the motor α on the rod i, i.e., $\mathbf{r}_i^\alpha = \mathbf{r}_{c,i} + x_i^\alpha \mathbf{u}_i$, i.e., the filament polarity is such that the motor head moves in the direction $\mathbf{u}_i$. The motor velocity v is a function of the loading force $\mathbf{F}_{m,i}^\alpha$ which builds up due to stretching of the motor tail. We use a force-velocity relation with a maximum value $v_{\max}$ for forces $\mathbf{F}_{m,i}^\alpha \cdot \mathbf{u}_i \geq 0$ pulling the motor forward, a linear decrease for forces $\mathbf{F}_{m,i}^\alpha \cdot \mathbf{u}_i < 0$ pulling the motor backwards, and $v = 0$ for $\mathbf{F}_{m,i}^\alpha \cdot \mathbf{u}_i < -F_{st}$, where F_{st} is the stall force [20, 21]. We assume that the motor binds to the filament when the distance between the position of the fixed end of the motor tail at $\mathbf{r}_0^\alpha$ and the filament is smaller than the capture radius w. Apart from the stall force F_{st} the motor is also characterized by its detachment force F_d, above which the unbinding rate of the motor head becomes large. For simplicity we assume in our model that the motor head detaches whenever the force $F_{m,i}^\alpha$ exceeds a threshold value F_d. We consider the case of processive motors with a high duty ratio close to unity, i.e., motors detach from a filament only if they reach the filament end or if the force F becomes larger than the detachment force F_d.

4.2 Simulation

Using the above model we performed simulations of gliding assays for a random distribution of motors with a surface density σ and periodic boundary conditions. At each time step Δt we update the motor head position x_i^α and filament position by using the discrete version of the equations of motion (5) and (6). The parameter values that we choose for the simulations are comparable with experimental data on assays for conventional kinesin. The simulation results presented in this article have been obtained for assays with quadratic geometry and size $25\mu m^2$ with rigid filaments of length $L = 1\mu m$ and diameter $D = L/40$. We simulate at room temperature $T = 4.28 \times 10^{-3} pN\,\mu m$. Friction coefficients are $\Gamma_\perp = 2\Gamma_\parallel = 4\pi\eta L/\ln(L/D)$ and $\Gamma_\theta = \Gamma_\parallel L^2/6$, where η is the viscosity of the surrounding liquid. We use a value $\eta = 0.5 pN\,s/\mu m^2$ much higher than the viscosity of water, $\eta_{\text{water}} \sim 10^{-3} pN\,s/\mu m^2$, which allows to take larger time steps and decreases the simulation time. We checked that this does not affect results. We use a maximum motor speed of $v_{\max} = 1\mu m s^{-1}$ and a stall force of $F_{st} = 5pN$. The capture radius for motor proteins is $w = 10^{-2}\mu m$ and the length of the fully stretched motor tail $L_m = 5 \times 10^{-2}\mu m$.

The motion of a *single* filament with contour length L is characterized by stochastic switching between rotational and translational diffusion if no motors are attached, directed translation in rotationally diffusing directions if one motor is attached, and directed translation in one direction if two or more motors are attached. The relative frequency of these types of motion depends on the mean number of motors attached to the filament or the mean distance $\langle d_m \rangle$ between bound motors and, thus, on the surface motor concentration

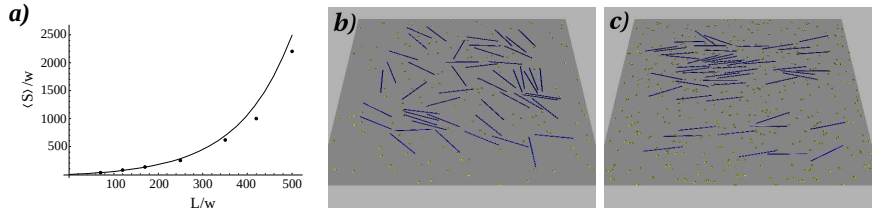

Fig. 4. (a) Simulation results for average distance $\langle S\rangle$ traveled by a filament between successive rotations as a function of the filament length L for high motor concentration. The solid line is the analytical result (7) as derived in Ref. [14]. (b) and (c): Snapshots of a gliding assay of rodlike filaments with filament density $\rho = 2/L^2$ on a motor coated substrate with randomly distributed motors and periodic boundary conditions. For detachment forces $F_d = F_{st}$, we find (b) an isotropic phase at low motor surface density $\sigma w L = 0.03$ and (c) active nematic ordering at high motor surface density $\sigma w L = 0.09$.

σ [14]. In the limit of high motor concentration a filament has two or more bound motors on average and $\langle d_m\rangle \sim 1/\sigma w$. The single filament performs a persistent walk with a persistence length [14]

$$\xi_p = \frac{\langle S\rangle}{\langle \Delta\theta^2\rangle} = \frac{1}{\langle \Delta\theta^2\rangle}\frac{L+2\langle d_m\rangle}{L+3\langle d_m\rangle}\frac{\langle d_m\rangle^2}{L}\left(e^{L/\langle d_m\rangle} - 1 - \frac{L}{\langle d_m\rangle}\right) \qquad (7)$$

where $\langle S\rangle$ is the mean distance traveled by a filament between successive rotations and $\langle \Delta\theta^2\rangle^{1/2} = 3\sigma/\sigma L^2$ the mean angle at rotations. The theoretical result (7) is confirmed by our simulation as shown in Fig. 4a. The mean filament velocity $v_F = \langle|\dot{\mathbf{r}}_{c,i}|\rangle$ can be obtained by simultaneously equating the filament friction force with the total motor driving force and the filament velocity with the motor velocity in the steady state, which gives $v_F = v_{\max}(1+\Gamma_\parallel v_{\max}\langle d_m\rangle/LF_{st})^{-1}$. This relation is confirmed by our simulations.

Our results for the simulation of *many* filaments with hard-core interactions indicate that the motility assay exhibits *active nematic ordering* if the motor density σ is increased as can be seen in the two simulation snapshots Figs. 4b and c.

References

1. A. Ott, M. Magnasco, A. Simon, and A. Libchaber, Phys. Rev. E **48**, R1642 (1993); J. Käs, H. Strey, and E. Sackmann, Nature **368**, 226 (1994).
2. F. Gittes, B. Mickey, J. Nettleton, and J. Howard, J. Cell Biol. **120**, 923 (1993).
3. J. Kierfeld, T. Kühne and R. Lipowsky, Phys. Rev. Lett. **95**, 038102 (2005).
4. J.R. Bartles, Curr. Opin. Cell Biol. **12**, 72 (2000).
5. K.R. Ayscough, Curr. Opin. Cell Biol. **10**, 102 (1998); S.J. Winder, *ibid.* **15**, 14 (2003).

6. M. Tempel, G. Isenberg, and E. Sackmann, Phys. Rev. E **54**, 1802 (1996).
7. O. Pelletier, E. Pokidyshevam L.S. Hirst, N. Bouxsein, Y. Li, and C.R. Safinya, Phys. Rev. Lett. **91**, 148102 (2003).
8. M.L. Gardel, J.H. Shin, F.C. MacKintosh, L. Mahadevan, P. Matsudaira, and D.A. Weitz, Science **304**, 1301 (2004).
9. J. Kierfeld and R. Lipowsky, Europhys. Lett. **62**, 285 (2003); J. Phys. A: Math. Gen. **38**, L155 (2005).
10. S.S. Sheiko and M. Möller, Chem. Rev. **101**, 4099 (2001).
11. N. Severin, J. Barner, A. A. Kalachev and J.P. Rabe, Nano Lett. **4**, (2004) 577.
12. P. Kraikivski, R. Lipowsky, and J. Kierfeld, Europhys. Lett. **66**, 763 (2004); Eur. Phys. J. E **16**, 319 (2005); Europhys. Lett. **71**, 138 (2005).
13. J. Scholey, *Motility assays for motor proteins*, Meth. Cell Biology **39**, (Academic Press, New York, 1993).
14. T. Duke, T.E. Holy, and S. Leibler, Phys. Rev. Lett. **74**, 330 (1994).
15. M.R. Faretta and B. Basetti, Europhys. Lett. **41**, 689 (1998).
16. F. Gibbons, J.-F. Chauwin, M. Despósito, and J.V. José, Biophys. J. **80**, 2515 (2001).
17. J. Howard, *Mechanics of Motor Proteins and the Cytoskeleton* (Sinauer Associates, Inc., Sunderland, 2001).
18. M.Doi and S.F.Edwards, *The Theory of Polymer Dynamics* (Clarendon, Oxford, 1986).
19. M. Warner and P.J. Flory, J. Chem. Phys. **73**, 6327 (1980); A.R. Khokhlov and A.N. Semenov, J. Stat. Phys. **38**, 161 (1985).
20. C. M. Coppin, D. W. Pierce, L. Hsu, R. D. Vale, Proc. Natl. Acad. Sci. USA **94**, (1997) 8539.
21. S. M. Block, C. L. Asbury, J. W. Shaevitz, M. J. Lang, Proc. Natl. Acad. Sci. USA **100**, (2003) 2351.
22. P. Kraikivski, R. Lipowsky, and J. Kierfeld, Phys. Rev. Lett. **96**, 258103 (2006).
23. The model can be extended to deformable filaments by modeling each filament as a set of N_s segments connected by elastic springs and hinges, see P. Kraikivski, Ph.D. thesis, Universität Potsdam, 2005.
24. J. Kierfeld, O. Niamploy, V. Sa-yakanit, and R. Lipowsky, Eur. Phys. J. E **14**, 17 (2004).